Materials and Structures (2023) 56:173
https://doi.org/10.1617/s11527-023-02256-z

ORIGINAL ARTICLE

Analytical and experimental shear evaluation of GFRP-reinforced concrete beams

Fausto Mistretta · Mario Lucio Puppio · Guido Camata · Antonio Nanni

Received: 4 June 2023 / Accepted: 2 October 2023

Abstract Reinforced Concrete (RC) technology is advancing towards new frontiers enhancing its sustainability and durability through innovative materials. In particular, the application of Glass Fiber Reinforced Polymer (GFRP) bars, in lieu of steel reinforcement, shows excellent performance, especially in aggressive environments. Nevertheless, current international design guidelines and standards tend to be rather conservative, especially concerning shear reinforcement. This element hinders the technology's competitiveness, not only in terms of material consumption but also in construction efficiency. This research aims to conduct an analytical comparison and experimental validation of the formulations found in some international standards pertaining to shear capacity in a specific case. The focus is on scenarios involving reduced shear reinforcement and cases where the number of stirrups falls below the minimum recommended by these standards. In the sample beam tests, two distinct flexural GFRP reinforcement ratios were employed to evaluate their influence on shear capacity, leading to diverse failure mechanisms: rupture of longitudinal GFRP bars and concrete crushing. The experimental results were used to compare the North American ACI, French AFGC, and Italian CNR shear capacity design approaches in the case of reduced transversal reinforced ratio. Analytical capacity expressions of the standards above are discussed with some remarks aiming at structural optimization.

Keywords GFRP · Reinforced concrete · Shear tests · Shear capacity models

List of symbols

A_f^+	Area of longitudinal reinforcement in tension
A_{fw}	Area of transverse reinforcement
b_w	Width of the web of the section
d	Distance from extreme compression fiber to the centroid of tension reinforcement
$C_{Rd,c}$	Factor according to AFGC (and EC2) and equal to 0.18/ γ_c
k, k_{cr}	Factor according to ACI (see "Equation" section in "Appendix")

F. Mistretta · M. L. Puppio (✉)
Department of Environmental Civil Engineering and Architecture, University of Cagliari, Cagliari, Italy
e-mail: mariol.puppio@unica.it

F. Mistretta
e-mail: fmistret@unica.it

G. Camata
Department of Engineering and Geology, Gabriele D'Annunzio" University, Chieti, Pescara, Italy
e-mail: guido.camata@unich.it

A. Nanni
Department of Civil and Architectural Engineering, University of Miami, Coral Gables, FL, USA
e-mail: nanni@miami.edu

Published online: 03 November 2023

e	Eccentricity—horizontal distance by point of load and the axis of the restraints in the test setup
E_i	Young modulus of the i-th material
H	Height of the section
M	Bending capacity
n_{fs}	FRP/steel young modulus ratio = E_f/E_s
n_{fc}	FRP/concrete young modulus ratio = E_f/E_c
f_c	Concrete compressive strength
f_{ct}	Concrete tensile strength, f_{ct} = 0.3*fc^(2/3) is the concrete tensile strength according to Italian Standard for Construction (NTC 2018)
f_f	FRP tensile strength of straight bars
f_{fr}	FRP reduced tensile strength of bent bars
r_b	Bending radius of the FRP stirrups
s	Stirrups spacing
τ_R	Shear strength
V	Shear capacity of the section
V_c	Shear capacity of the concrete compressive section
$V_{c,\max}$	Maximum shear capacity of the concrete compressive section due to the failure of the strut
V_f	Shear capacity of the FRP stirrups
V_s	Shear capacity of the steel stirrups
α_b	Strength reduction factor for bending effect
α_E	Strength reduction factor of elastic modulus E (also indicated as "strain limitation" in literature)
β_1	Factor is taken as 0.85 for concrete strength fc′ up to and including 28 MPa. For strength above 28 MPa, this factor is reduced continuously at a rate of 0.05 per every 7 MPa of strength over 28 MPa but is not taken less than 0.65.
γ_i	Safety factor according to AFGC, CNR
$\gamma_{f,\Phi}$	Safety factor for stirrups according to CNR DT203/2006 (assumed equal to 0.5)
δ	Vertical displacement
ε_{cu}	Ultimate deformation of concrete in compression
θ	Inclination of the strut
λ_s	Factor according to ACI 440.11-22 (see "Equation" section in "Appendix")
ρ_f	$A_f^+/(b_w d)$—Longitudinal reinforcement ratio
ρ_{fb}	Longitudinal reinforcement ratio (in tension) producing balanced failure
τ_R	$0.25 f_{ct}$—Shear resistance according to CNR DT203/2006
τ	Average shear strength, Average shear strength of the concrete section calculating as $V/(b_w * d)$
Φ	Safety factor according to ACI

Subscript

a	Average
c	Concrete
d	Design
e	Expected
exp	Experimental
k	Characteristics
f	FRP
n	Nominal
s	Steel
u	Ultimate

Note of the authors

d *Design* Values, according to a certain standard, are based on characteristic values of strength with the application of safety factors.

e *Expected* Values are based on the average value of strength without safety factors. Expected values are used to interpret *experimental (exp)* data.

As utilized in this paper, the symbols and equations from ACI, AFGC, and CNR [1–4] have been harmonized to facilitate a more effective comparison of the standards and enhance text readability. They are summarized above.

1 Introduction

Composites gradually entered the history of concrete construction, first as retrofit reinforcements and later as reinforcing bars for new constructions [5]. Fiber Reinforced Polymers (FRP) bars are particularly interesting for structures exposed to aggressive environmental conditions, such as coastal structures, ports, bridges, and industrial facilities [6–9]. The Glass Fiber Reinforced Polymer (GFRP) technology is gaining increasing interest, driven by the rising cost of steel and the improvements in life cycle performance that composites can offer, coupled with ongoing enhancements in the production chain. In the history of RC structures, the analysis of shear capacity evolved with the following main steps. Following Jourawsky's

theory (for homogeneous, elastic, and uncracked beams, with the limitation of the shear stress), the first design method for the cracked beam is represented by the truss-model, well-known as Ritter–Mörsh (R–M) trellis theory. In this, the check of tensile action in stirrups (V_s) and compressive action in concrete struts ($V_{c,max}$) determines the capacity of the members. This model does not assign any shear resistance to the compressed concrete area (area of the horizontal strut of a RC beam). An important parameter in the R-M model is the inclination of the compressed strut, usually indicated as θ, that identifies the trellis and consents to consider it statically determined together with the hypothesis of uniform plasticity of the stirrups. With this hypothesis, R-M model also takes the name of the "simplified truss model" or "plastic truss analogy".

A further step actually used in ACI and most modern code is represented by Eq. (1):

$$V = V_c + V_s \tag{1}$$

In this, the contribution of the concrete V_c in compression is summed up to the contribution of the stirrups V_s. In the beginning, the expression of V_c was experimentally derived as an extrapolation of experimental data while the contribution of stirrups V_s was derived by the R-M model, with the limitation of $\theta = 45°$. The progress obtained with experimentation consented to express V_c as a function of the mechanical parameter of the concrete sections. In this path the check of the resistance of the compressed struts is implicitly considered in a reduction of V_c and the coexistence of V_c and V_s in a unique expression is obtained by a limitation of tensile stress and strain in the stirrup as well as considering $\theta = 45°$. Other methods are based on the Compression Field and Shear Friction Theory. Compression Field Theory is based on the first work of Collins and Mitchel [10]. This constitutes the basis of the first version of the Canadian Concrete Code and had some conceptual modifications from 1984 to 2004. The Shear Friction theory focuses on the shear friction of slender elements. Except for the R-M model, all these methods are based on Eq. (1) and present a different expression for V_c.

Equation (1), now applied in ACI for ordinary concrete members, is modified to calculate the resistance of RC-FRP members considering the different mechanical properties of FRP with respect to steel. As best explained in Sect. 2 the expression for V_c usually derives from the one used for ordinary RC members with some modification to consider the different mechanical characteristics of FRP bars. In FRP-RC, as for conventional steel-RC, the concrete contribution to the shear strength (V_c) includes, directly or indirectly, uncracked concrete and aggregate interlock. Dowel action, developed by the longitudinal reinforcement, is usually neglected because of the orthotropic behavior of FRP bars [11, 12]. The contribution of stirrups or of the transverse reinforcement (V_s of steel becomes V_f for FRP members) is typically estimated using the truss analogy with $\theta = 45°$ and is summed up to V_c. This except for the French standards that consent to consider the maximum value between V_c and V_f, depending, the latest, on the inclination of the compressed strut θ. In this case, V_f assumes the following value:

$$V_f = \frac{A_{sw}}{s} d f_{fr} \cot\theta \tag{2}$$

So in AFGC the term V_f can be increased up to 2.5 by the terms $\cot(\theta)$ but is penalized by the reduction of resistance of stirrups f_{fr} as best expressed in the following Table 3.

Even though research on the shear performance of FRP-RC members is an active topic of investigation, a comprehensive list of works preceding 2015 was published by Razaqpur and Spadea [13] and, before them, by Tureyen and Frosch 2003 [14]. This list includes more than 300 shear test results for FRP-RC beams, many of which were conducted on small-scale rectangular cross-section specimens. Fico et al. (2007) in "Assessment of Eurocode-like design equations for the shear capacity of FRP RC members" [15] presents an extensive comparison of Canadian CSA S-802, American ACI 440.1R, Italian CNR-DT 203, and Japanese JSCE expression for shear capacity for FRP-RC beams. The analysis is based on a wide database of beams with and without shear reinforcement. The paper analyzes the key points of the shear design of FRP prototypes and is a milestone in the state of the art presenting the assessment of Eurocode-like equations and introducing the actual basis of Italian standard. Fico et al. proposed a model that considers strain limits for stirrups contribution (0.0035 for CFRP, 0.0070 for AFRP, and 0.0085 for GFRP). Oller et al. [16] developed a simple and rational model for the shear capacity of FRP-RC beam. The model is based on the

coexistence of the following three mechanisms: shear force in the uncracked concrete chord, tensile strength along the crack length, and shear strength of the transverse reinforcements. The expression of Oller et al. is applied to a database of 112 shear tests on FRP-RC beams producing interesting results considering the mean value (1.08) and the relative coefficient of variation (19.5%). The paper also presents a wide comparison of the actual standards including, but not limited to, the model proposed by other authors like Fico et al. Hegger et al. and Nehdi et al. [17]. The model proposed in the aforementioned works exhibits the lowest coefficient of variation among all the analyzed models. This holds significant importance because this model is grounded in the principles of structural mechanics. Mukhtar and Deifalla [18] proposed some modifications of the Critical Shear Crack Theory (CSTC) based on the analysis of 420 experimental tests of FRP-RC deep beam without stirrups. This results in two versions of CSTC called Modified Critical Shear Crack Theory (MCSTC). MCSTCI and MSCTCII are hybrid models, based on a well-known physical based model with an extensive empirical fitting. It is interesting to emphasize that shear capacity is expressed here as a function of slenderness ratio (a/d) besides elastic modulus ratio (Es/Ef). These models are validated by the authors on a blind set of experimental data and compared with the results furnished by international standards producing interesting results. In terms of shear capacity prediction, empirical expressions for the concrete contribution to shear were proposed and adjusted to account for the elastic modulus ratio between steel and FRP bars [19, 20]. In other instances, experimental evidence of the shear performance of FRP-RC beams was used to develop empirical or semi-empirical expressions using tailored parameters [21, 22]. Other works have considered mechanistic models based on the modified compression field theory for the prediction of the shear strength of FRP-RC members providing a more rational approach to design [23, 24]. Finally, more recent works have implemented optimization approaches to predict the shear strength of FRP-RC elements. For example, Nehdi et al. [17] and Ebid et al. [25] produced equations that include optimal parameters to minimize errors. Similarly, other studies have focused on machine learning [26] and deep learning [27], creating models based on large datasets to account for a wide variety of parameters. These models, although very accurate for predictive use, do not appear to have immediate application for design purposes.

It is well known that the post-cracking behavior of beams reinforced with FRP bars differs from that of beams reinforced with traditional steel bars [28]. This is essentially due to the linear-elastic behavior of FRP bars, their anisotropy, reduced axial stiffness [29], and their bond behavior [30, 31]. The FRP-RC beams exhibit larger and deeper cracks compared to steel-RC beams. While there is substantial agreement on bending capacity in the technical literature, the expressions for shear capacity are rather conservative and produce scattered results [32]. For this reason, this research focuses on the shear behavior of GFRP-RC beams. The two sample beams designed herein are characterized by a limited stirrups amount and two salient bending reinforcement ratios. A highlight of the scope and aim of the paper is therefore presented here:

- Experimental tests are carried out on beams with a reduced stirrups amount and with different bending reinforcements (under-reinforced and over-reinforced),
- –ACI, AFGC, and CNR standards expressions are applied to the case study presented here to assess their predictive capabilities. It's important to note that, since the number of stirrups falls below the minimum allowable, both prototypes mentioned should be analyzed as beams without explicit shear reinforcement. The question is whether these models can accurately predict the experimental results.
- The position [$\cot(\theta) = 1$] in ACI and CNR, typically assumed when considering concrete strength in conjunction with stirrups strength, along with the "strain limitation" (referred to in this work as coefficient α_E), is compared to the experimental results;
- A parametric analysis of the expression of ACI, AFGC, and CNR is carried out providing enhancing insight into the current performance requirements, especially the strain limitation in stirrups,
- A fem modeling is tuned on the experimental test carried out to contribute to a better understanding of the shear behavior of FRP-RC prototypes.

Specifically, the two main types of failure obtained (FRP rupture and concrete crushing) are investigated

considering the sectional approach of four selected North American and European standards; analytic shear capacity expressions of the ACI 440.1 R15 [1] and ACI 440-22 [2], AFGC [3] and CNR, [4] are examined and compared to the outcomes of experimental tests.

2 Capacity models

International standards offer multiple expressions to assess the capacity of FRP RC beams. Fib Bulletin 40 [33] provides a comprehensive discussion of the shear capacity of concrete beams reinforced with FRP bars. In "FRP Reinforcement of RC Structures," the authors extensively review key contributions in this field. They highlight how formulations from various international standards, such as the Japanese JSCE, British design codes BS8110, American ACI, Canadian CSA, and Italian CNR, initially tailored for ordinary steel-reinforced concrete, were modified to account for the unique rheological behavior of FRP bars, resulting in current expressions. Notably, Guadagnini et al. introduced a design approach that suggested increasing the deformation limit of stirrups to 0.0045 for both shear and flexural reinforcements (originally assumed to be 0.002, corresponding to steel yielding). Today, this recommendation has been incorporated into some current standards, with ACI and AFGC now proposing a limit of 0.005. Some other interesting remarks are worthy of attention: the approach of variable strut angle, the only shear design method adopted in Eurocode 2, thus ignoring the concrete contribution for members with shear reinforcements, is adopted from the French AFGC standard joined with a deformability limit of 0.005. From the other side, FIB Bulletin 40 recommends the simplified fixed strut angle, with $\cot(\theta) = 1.0$, in the case the concrete strength is considered together with transverse reinforcements.

The different approaches were investigated by applying them to both the sample beams tested here. In this paper, the focus is on the failure caused by the combination of tension in the stirrups and the shear failure of the compressed concrete zone shown in Fig. 4. The Shear capacity of RC-FRP elements V is obtained by the sum of tangential stress acting on the concrete compressive section V_c added to the contribution of the FRP stirrups in tension V_f, as in Eq. (3).

$$V = V_c + V_f \tag{3}$$

As anticipated in the introduction, whereas North American and Italian shear capacity expression [1, 2, 4] considers the sum of V_c and V_f, The French AFGC [3] does not admit to summing together these two values but, unlike the other standards, takes into account the inclination of the strut θ in V_f. The reduced resistance of the FRP stirrups (f_{fr}) derives from the tensile strength of the straight bar, which is penalized to consider the bent effect, to limit the crack width, and to reduce the effects of fatigue in GFRP stirrups (especially for bridges). The expressions for f_{fr}, V_c, and V_f are listed in Table 1.

To simplify the comparison of the equations in Table 1 the unified symbols indicated in the

Table 1 Shear capacity according to [1–4]

	f_{fr} [b]	V_c	V_f
ACI 440.1R-15	$\min\begin{cases}\alpha_b \cdot f_f \\ \alpha_E \cdot E_f \le f_f\end{cases}$	$\frac{2}{5}\sqrt{f_c} \cdot b_w(kd)$	$\frac{A_{fw} \cdot d \cdot f_{fr}}{s}$
ACI 440.11-22	$\min\begin{cases}\alpha_b \cdot f_f \\ \alpha_E \cdot E_f \le f_f\end{cases}$	$\max\begin{cases}2/5 \cdot \lambda_s \sqrt[2]{f_c} \cdot b_w(k_{cr}d) \\ 0.0664 \cdot \lambda_s \sqrt[2]{f_c} \cdot b_w d\end{cases}$	$\frac{A_{fw} \cdot d \cdot f_{fr}}{s}$
AFGC [a]	$\min\begin{cases}\alpha_b \cdot f_f \\ \alpha_E \cdot E_f \le f_f\end{cases}$	$C_{Rd,c}k\left(100\frac{E_f}{E_s}\rho_l f_c\right)^{\frac{1}{3}}b_w$	$\frac{A_{fw} \cdot d \cdot f_{fr}}{s}cot(\theta)$
CNR-DT203/2006	experimental tests or $\frac{f_f}{\gamma_{f,\phi}}$	$1,3 \cdot k\left(\frac{E_f}{E_s}\right)^{\frac{1}{2}}(1,2+40\rho_l)\tau_R b_w d$	$\frac{A_{fw} \cdot d \cdot f_{fr}}{s}$

[a] In AFGC, V_c and V_f contributions are not considered as acting together

[b] α_E assumes the value 0.004 in ACI 440.1R-15 and 0.005 in ACI 440.11-22 and AFGC

Symbols in the table are unified according to the list of symbols presented above

Table 2 Shear safety factors according to [1–4]

Standard	Percentile for characteristic distribution (%)		Factor		Values - Φ
ACI 440.1R-15	0.1		Φ - capacity		Φ = 0.75
ACI 440–22	0.1		Φ - capacity		Φ = 0.75
		Concrete - γ_c	FRP - γ_f (bending)		FRP - $\gamma_{f,r}$ (shear)
AFGC	5.0%	1/γ - strength	γ_c = 1.30	γ_f = 1.30	$\gamma_{f,r}$ = 1.30
CNR-DT203/2006	5.0%	1/γ - strength	γ_c = 1.50	γ_f = 1.50	$\gamma_{f,r}$ = 2.00

appendices were used. The average and characteristic values of the compressive strength of concrete $f_{c,}$ the tensile strength of concrete f_t, and the shear strength of concrete τ_r are indicated in Table 4. It's worth noting that there are distinct differences in the percentile values of characteristic strength distributions between the American ACI and the European AFGC and CNR standards ("Clarification" section "Appendix"). The strength of the GFRP bars depends on the diameter as well.

In CNR V_c is a function of τ_r, and $\tau_r = 0.25\, f_{ct}$ (being f_{ct} = 0.3*fc^(2/3)), while in the other technical standard V_c is a function of concrete compressive strength f_c. The forthcoming ACI 440–22 proposes two different expressions for V_c, depending on the longitudinal reinforcement ratio. V_f is calculated as the min of $f_{fr} = \alpha_E E_f$ and $f_{fr} = \alpha_b f_f$ in ACI and AFGC. The term α_E assumes the value 0.004 for ACI 440.1R-15 and 0.005 for ACI 440.11–22 and AFGC. The term α_b, which introduces the weakening effect due to the bending, can be determined with Eq. (4) [34], in which r_b is the bending radius and d_b is the bar's diameter. The AFGC is the only one that introduces cot(θ) in V_f expression, according to Eurocode 2 [35] for ordinary RC members. The inclination of θ is limited to 33° (cot(θ) = 1.5) according to the indication of AFGC (with the scope to reduce the effect of fatigue in the stirrups) whereas for ACI and CNR cot(θ) = 1.0 as also indicated in Table 1.

$$\alpha_b = \left(0.05 \cdot \frac{r_b}{d_b} + 0.3\right) \tag{4}$$

The Italian CNR expresses f_{fr} recommending the use of experimental results or with a "safety factor" $\gamma_{f,\Phi}$ = 2, while there are no restrictions on strain limitation (α_E).

Regarding safety factors (s.f.):

- The American approach considers a single coefficient ($\Phi < 1$) that affects nominal capacity, so the design value of shear capacity is obtained by the nominal value, calculated with the characteristics value of strength, multiplied by Φ.
- The European approach, according to EC2 [35], considers several coefficients ($\gamma_i > 1$) that affect strength, and thus the design value of shear capacity is obtained from the expression of Table 3 by dividing the respective characteristic strengths by γ_i.

The values of Φ and γ are summarized in Table 2, where expected (e) and design (d) values of concrete compressive strength f_c, shear strength—calculated according to Italian standard—τ_r, tensile strength of the straight FRP bars f_f and tensile strength of the bent FRP bars f_{fr} are mentioned (Table 3).

3 Experimental evidence

3.1 Design

The experimental activities are focused on four-point bending tests on beams with constant stirrups spacing equal to 0.8 times the height of the section h. The ongoing approaches on shear capacity are based on Eq. (3), where V_c is essentially related to the concrete resistance and longitudinal reinforcement ratio. To evaluate the effect of the latter on the shear capacity, two different beams were designed with a cross-section of 200 × 400 mm, equal stirrups spacing, and two different longitudinal reinforcement ratios.

As is commonly known, the quantity of longitudinal reinforcement plays a critical role in determining two distinct types of bending failure. In beams with limited bending reinforcement, often referred to as

Table 3 Expected and design values of strength

	Expected	Design
f_c	Average value without s.f	Characteristics values and s.f. according to the respective standard
τ_r	0.25 f_{cta} without s.f	0.25 f_{ctd} with s.f
f_f	Average value without s.f	Characteristics values and s.f. according to the respective standard
f_{fr}	Average value of the resistance of the stirrups (Table 4)	Characteristics values, s.f. en expression according to the respective standard (Table 3)

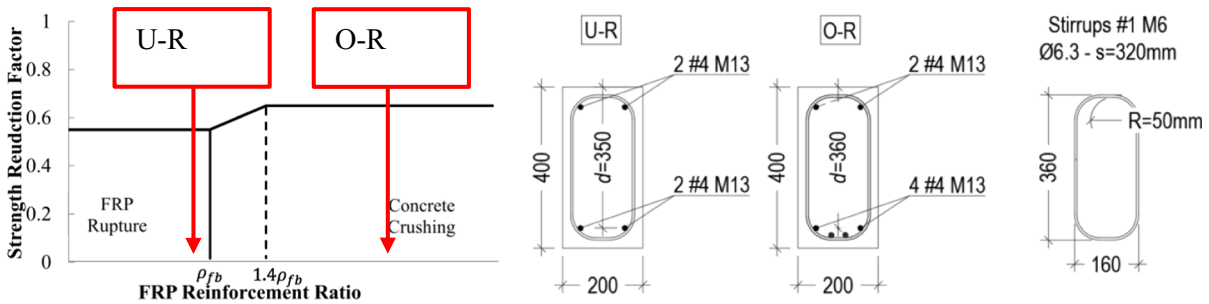

Fig. 1 Limit of reinforcement ratio ρ_{fb} vs strength reduction factors [1] and beam sections

Table 4 Properties of concrete and of the GFRP bars [37, 38]

Property	Average	Standard deviation
Concrete		
Elastic modulus—E_c	28.6 GPa	–
Compressive strength—f_c	34.5 MPa	1.8 MPa
Tensile strength—f_{ct}	3.7 MPa	0.4 MPa
Nominal tensile strength[1] (NTC2018)—$f_{ct,NTC}$	2.7 MPa	–
Nominal shear strength[1] (CNR)—τ_r	0.6 MPa	–
GFRP bars		
Elastic modulus—E_f	46.0 GPa	–
Tensile strength of the M13 bars—$f_{f\#4}$	979 MPa	51 MPa
Tensile strength of the M6 bars—$f_{f\#1}$	1007 MPa	47 MPa
Tensile strength of the M6 bent bars—f_{fr}	705 MPa	92 MPa

under-reinforced (U-R), failure occurs primarily due to the yielding and collapse of the tensile bars. Conversely, in sections with a substantial amount of reinforcement, known as over-reinforced (O-R), failure is typically associated with concrete crushing. These dual-limit behaviors are depicted in Fig. 1, which also delineates the transition zone between U-R and O-R. The sample beams in question were intentionally designed to exhibit U-R and O-R behaviors. However, it's important to note that both of these specimens were engineered to induce shear failure rather than bending failure, as elucidated below. The mechanical properties of concrete and GFRP bars are listed in Table 4. For the concrete, four compression tests, four indirect tensile tests, and two tests for elastic modulus are carried out. The value of tensile strength calculated with the Italian standard (§11.2.10.2 NTC2018) [36] is also presented, being the same value used to calibrate the capacity equation in CNR [4]. GFRP bar properties of straight bars were adopted from Kocaoz et al.[37], being in good agreement (but less prudential) with those reported by the

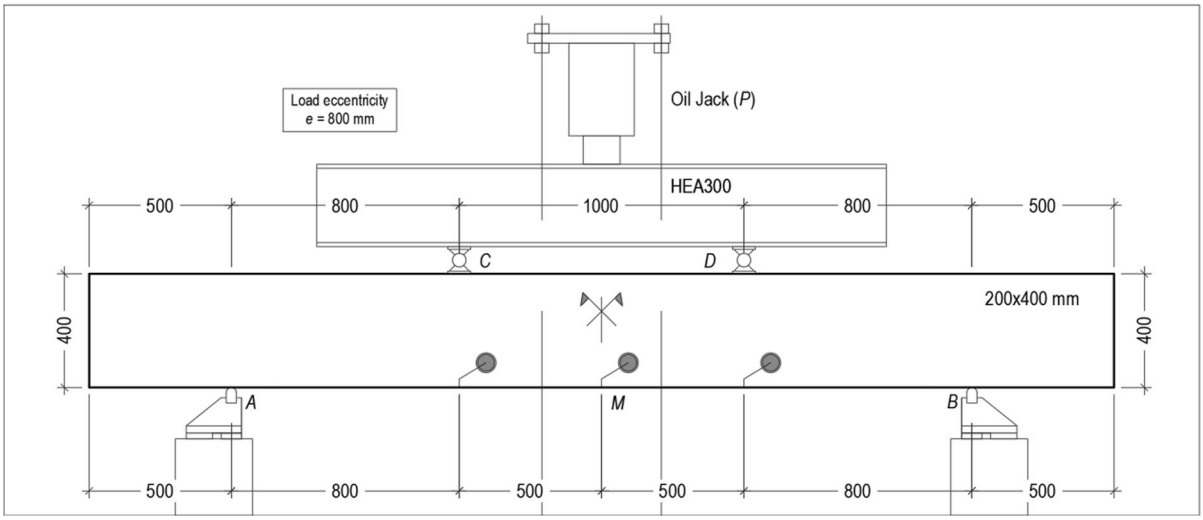

Fig. 2 Layout of the test and main dimension of the sample beams (mm)

manufacturer and in ASTM D7957 [38]. The reduced strength of the bent bars is experimentally calculated on six stirrups specimens according to ASTM D7914/D7914M-14.

O-R and U-R beams are based on ACI 440.1 R15 [1]. In particular the balanced failure conditions are furnished by (5):

$$\rho_{fb} = 0.85\beta_1 \frac{f_c}{f_f} \frac{E_f \varepsilon_{cu}}{E_f \varepsilon_{cu} + f_f} \tag{5}$$

where the symbols are listed in Notations. Equation (5) allows defining the so-called transition zone: when $\rho_f < \rho_{fb}$ the flexural failure is controlled by the reinforcement rupture, but when $\rho_f > 1.4\rho_{fb,}$ it is controlled by the concrete crushing. Two different flexural reinforcement ratios are selected (Fig. 1) to investigate their effect on shear capacity. The first one corresponds to Under-Reinforced (U-R) section with two #4 bars (M13). The second one corresponds to Over-Reinforced (O-R) section with four #4 bars (M13) as tensile reinforcement. In both cases, the compression reinforcement consists of two #4 (M13) bars. Figure 1 also shows the s.f. Φ that is used with the nominal bending resistance (M_n) to obtain the design resistance (M_d) according to [1]. Φ assumes two distinct values for U-R (0.55) and O-R (0.65) beams.

$$M_d = \Phi M_n \tag{6}$$

The two reinforcement ratios, smaller and larger than the balanced failure limit, are computed considering nominal diameters and are:

- U-R $\rho_f = 0.34\%$;
- O-R $\rho_f = 0.69\%$.

Taken the flexural capacity of the U-R beam ($M_{\min}$) and the shear arm of the beam being twice the height of the sections (e = 800 mm in Fig. 2), the shear capacity V, in order to obtain shear failure, must be:

$$V < M_{\min}/e \tag{7}$$

From this, the transverse reinforcement area A_{sw} = 62.3 mm^2, with a spacing of 320 mm (A_{sw}/s = 0.190 mm^2 / mm) is chosen for both beams as depicted in (Fig. 1). The shear reinforcement is the same for both the beams thus, the only difference in ρ_f. It is observed that these values of A_{sw}/s_w are below the limits (Table 5) specified by the selected standards [1–4]. The execution of the beams and the experimental tests were conducted at the Material Testing Laboratory of the University of Cagliari.

With #1 two arms stirrups the minimum spacings to be considered in the design, according to AFGC, is 172 mm. The spacing used in this experimental campaign is 1.86 times the minimum value required by AFGC and slightly higher than the value provided by CNR (310 mm). With this spacing (s = 320 mm) shear capacity should be calculated as the only

Table 5 A_{sw}/s, minimum transverse reinforcement ratio and s_{min} minimum stirrups spacing with #1 two arms stirrups [1–4]

	ACI 440.1R-15	ACI 440.11-22	AFGC	CNR 203 2006
A_{sw}/s	0.320 mm^2/m $0.06\sqrt{f_c'}\frac{b_w}{f_{fr}}$	0.250 mm^2/mm $0.06\sqrt{f_c'}\frac{b_w}{f_{fr}}$ $0.35\frac{b_w}{f_{fr}}$	0.360 mm^2/mm $0.08\frac{\sqrt{f_c'}b_w}{0.0045\cdot E_{FRP}}$	0.230 mm^2/m $0.06\sqrt{f_c'}\frac{b_w}{0.5\cdot f_{fr}}$
s_{min} (#1–2 arms)	196 mm	245 mm	172 mm	310 mm

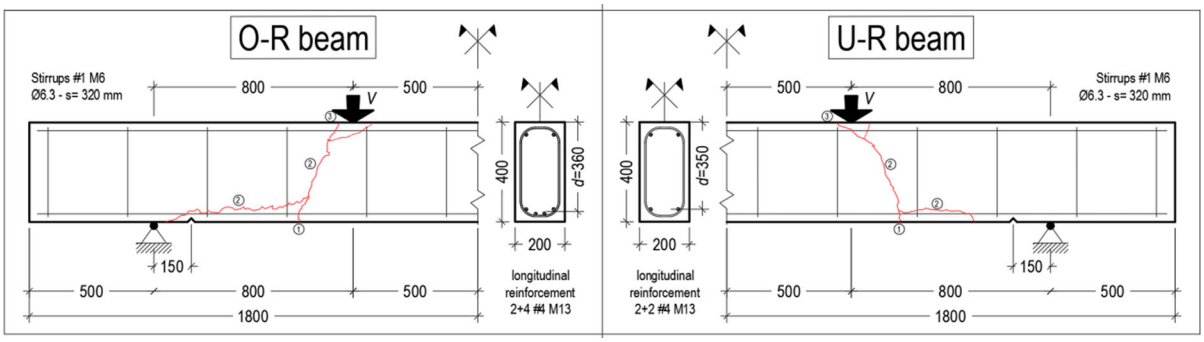

Fig. 3 Reinforcement of the two specimens and test setup. The red line highlights the path of the shear cracking and the numbers from 1 to 3 its evolution during the experimental test, involving two stirrups for O-R and one stirrup for the U-R specimen

contribution of V_c. The mechanical accuracy of this assumption is best discussed below.

3.2 Experimental setup and test results

The test setup is described in Fig. 2. Six LVDT transducers were placed at sections *C*, *M*, and *D*, at the intrados of the beam, three on each side. The load (*P*) was applied using a hydraulic jack. Load application points were placed with a shear arm e = 800 mm (Fig. 3) having in a ratio e/d = 2.2.

The load *P* from the hydraulic jack was applied until the failure was reached. The relative V-δ ($V = P/2$) curve is presented in Fig. 8. The displacement (δ) in section *M* (the average from the front and rear displacements) is used in these plots. It should be noted that the shear crack at collapse intersected at least one stirrup (Fig. 4). A different inclination of the compressed strut for the two specimens is observed. The first crack (numbers from 1 to 3 in Fig. 3) presents an inclination of about 60° for the UR and 50° for the OR beam. Then, after the formation of progressive sub-horizontal cracking due to loss of adherence, the compressed strut re-orients itself involving the adjacent stirrups in the failure mechanism. The geometry of the systems limits the terms $\cot(\theta)\cdot d/s$ to the maximum value 2, being 2, the maximum number of stirrups that can be involved in the failure mechanism.

So, the initial diagonal cracks (1 in Fig. 3) are joined with a pseudo horizontal one (2 in Fig. 3, more developed in the case of OR, as expected) that highlights loss in adhesion of horizontal reinforcements. It should be noted that the shear crack at collapse intersected at least one stirrup (Fig. 4). The evidence that diagonal cracks are joined with a pseudo-horizontal one (more developed in the case of OR, as expected) highlights a loss in adhesion of horizontal reinforcements. For the O-R beam, after the opening of a large diagonal crack, collapse is obtained for the crushing of the compressive concrete area (Fig. 4). In the U-R beam, final failure occurred due to the rupture of the longitudinal bars, which happened with the complete cracking of the section, the stirrup failure, and 24 mm of deflections. In the case of U-R beams the final collapse is obtained with the failure of longitudinal reinforcement, which happened after the

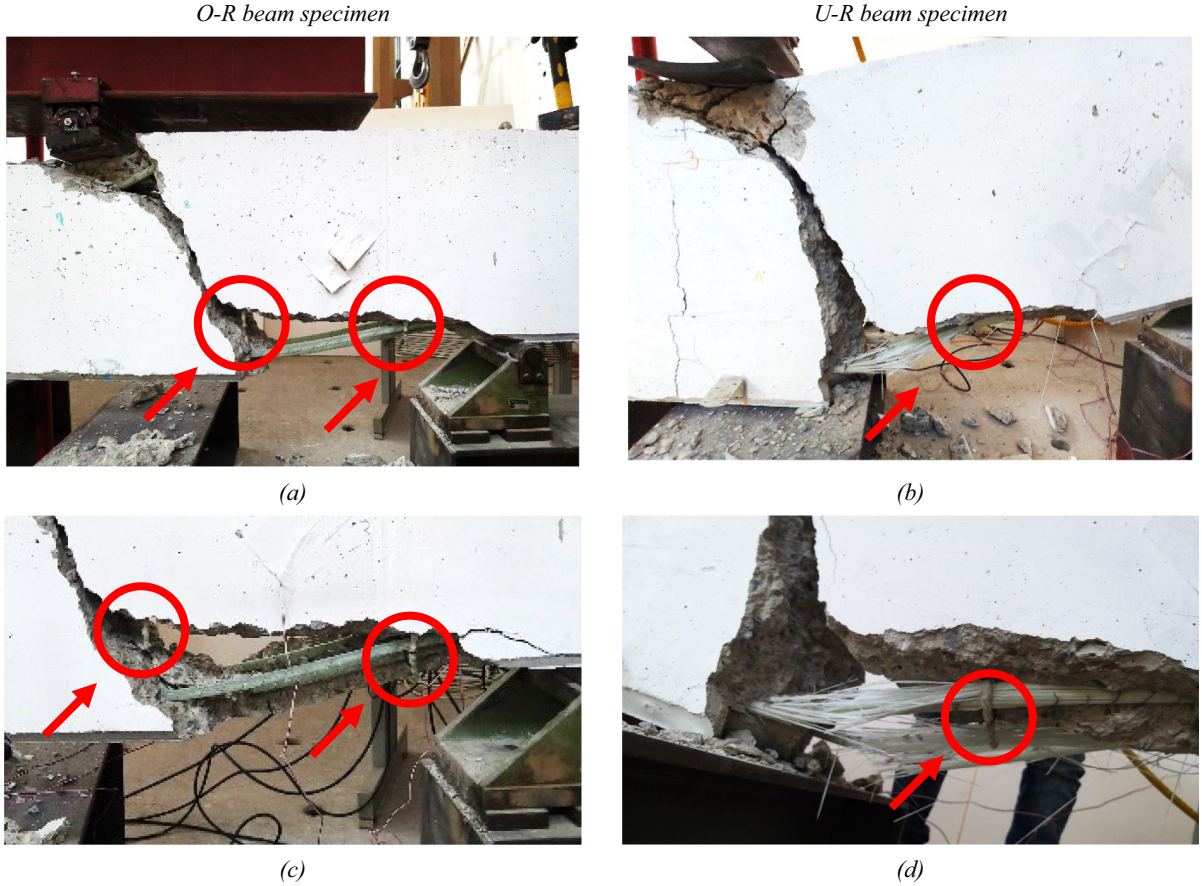

Fig. 4 Failure of O-R (**a**, **c**) and U-R (**b**, **d**) beams and detail of the respective intrados (c and d). Red arrows and circles indicate the failed stirrups

complete cracking of the section, stirrup failure (Fig. 4), and 45 mm of deflections (Fig. 8).

In Fig. 5 the shear capacities V are calculated according to the mentioned standards. V_e is the expected value, calculated without the safety coefficient and with the average value of strength, whereas V_d is the design value, calculated with the safety coefficient (Table 2) and the characteristics values. V_{exp} is the experimental value. It should also be highlighted that the use of $f_{fr} = \alpha_b \cdot f_{fb}$, with α_b from Eq. (4) [34], furnished in this case $\alpha_b = 0.7$ with and $f_{fr} = 705$ MPa, is close to the value experimentally determined. Table 4 shows a different ratio of V_c/V, V_f/V *and* V/V_{exp} for the analyzed standard (Table 6).

The comparison between the bending capacity expression is presented in Fig. 6. The examined standards agree on the bending, showing a reduced variation of M. It is observed that the moment M for which shear failure occurred (green line in Fig. 2) is less than the expected value from the analytic formulation. This is consistent with the design assumptions/hypothesis to obtain shear failure for both specimens. The position of the y-axis of balanced failure is used in the case of U-R and the iterative procedure is used to calculate y for the O-R specimen. In both cases, the upper reinforcement is neglected in the calculation for safety.

3.3 Numerical model

The experimental campaign was studied with sophisticated 3D nonlinear finite element models using the programs STKO [39] and *OpenSees* [40]. Figure 5a shows the mesh discretization and the boundary conditions. The model uses the condition of symmetry to reduce the number of degrees of freedom. The

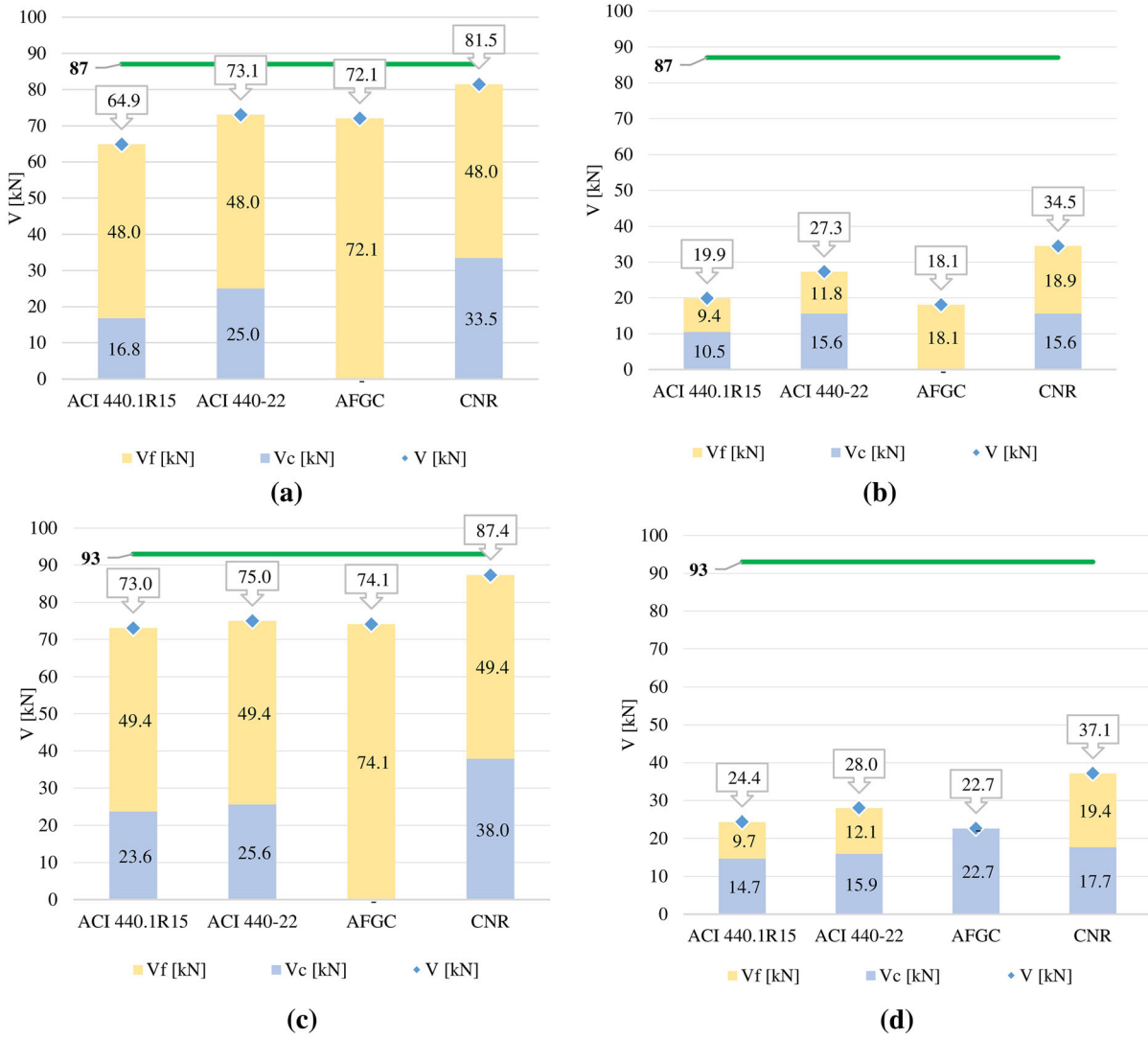

Fig. 5 Shear capacity for U-R section, Expected (**a**) and Design (**b**) values, and for O-R section, Expected (**c**) and Design (**d**) values. The green line represents experimental results

beams are discretized with four node tetrahedron elements and the rebars with displacement beam columns with fiber sections. Concrete is modeled with the ASDConcrete3D constitutive low using an IMPL-EX integration scheme [41, 42] and the longitudinal rebars and stirrups with a linear elastic material. The bond is modeled according to experimental data of G-FRP from Aiello et all. [30] that carried out bond tests on Glasspree type bars (Sireg, Italy); the same bars, and with the same surface finishing, were used in the experimental campaign. The material properties are those listed in Tab 4. The concrete tensile fracture energy is calculated using CEB FIB Model Code 2010 [43], and the compressive fracture energy is assumed to be 250 times the tensile fracture energy. The comparison between the numerical and experimental load–displacement curves shows very good agreement as shown in Fig. 6. The numerical failure mode of the two beams confirms the experimental findings (Fig. 5b and c). The numerical model shows that the O-R beam failed because of excessive stresses in the straight part of the stirrups and concrete crushing, and the U-R failed because of the longitudinal bar tensile failure [41] (Figs. 7, 8).

Table 6 V_c/V, V_f/V, and V_{exp}/V for U-R and O-R beams

	Expected			Design		
	V_c/V (%)	V_f/V (%)	V/V_{exp} (%)	V_c/V (%)	V_f/V (%)	V/V_{exp} (%)
U-R beam						
ACI 440.1 R15	26	74	75	53	47	23
ACI 440.11–22	34	66	84	57	43	31
AFGC	0	100	83	0	100	21
CNR	41	59	94	45	55	40
O-R Beam						
ACI 440.1 R15	32	68	79	60	40	26
ACI 440.11–22	34	66	81	57	43	30
AFGC	0	100	80	0	82	24
CNR	43	57	94	48	52	40

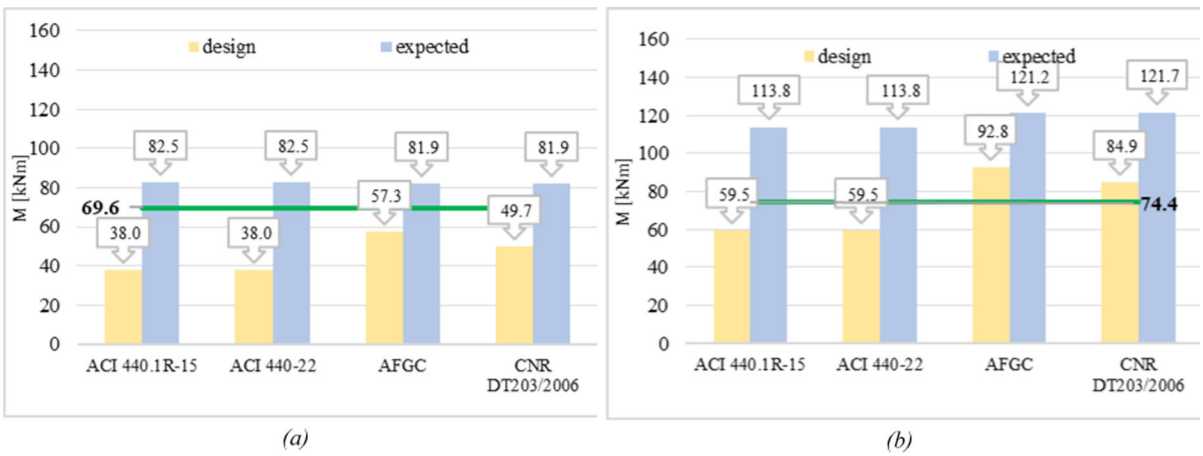

Fig. 6 Bending capacity of U-R (**a**) and O-R (**b**) beam. The horizontal line represents the bending value corresponding to the shear collapse

4 Parametric analysis and discussion

This work investigates the shear behavior of beams with a reduced percentage of transverse reinforcement, lower than the limits provided by the mentioned Technical Standard [1–4]. Two sample beams (U-R and O-R) are tested to obtain shear collapse. The analytical formulations furnished by technical standards were examined by calculating both the Expected (subscript *e*) value and the Design (subscript *d*) value of capacity and comparing it with the Experimental data (subscript *Exp*). The analytic formulations of ACI, AFGC, and CNR were also used to calculate the bending M and shear capacity V of the U-R and O-R beams. The respective average values, standard deviations, and percentage deviations of the considered standard are shown in Table 7.

Bending capacity M presents a reduced percentage deviation (up to 21% for U-R and from 4 to 23% for O-R). Shear capacity V presents a greater percentage deviation (from 9% up to 30 for U-R and from 9 to 23% for O-R). The more significant variation depends on the different assumptions on strength and the safety factors used by the different standards and is obtained in the case of design values. The greatest dispersion is found in the case of design, produced by the incidence of the safety coefficient and in the different assumptions in the calculation V_c and V_f. The variation of V_f is significantly related to the different assumptions made for f_{fr} (as also shown by the fact that V_{fe}, calculated

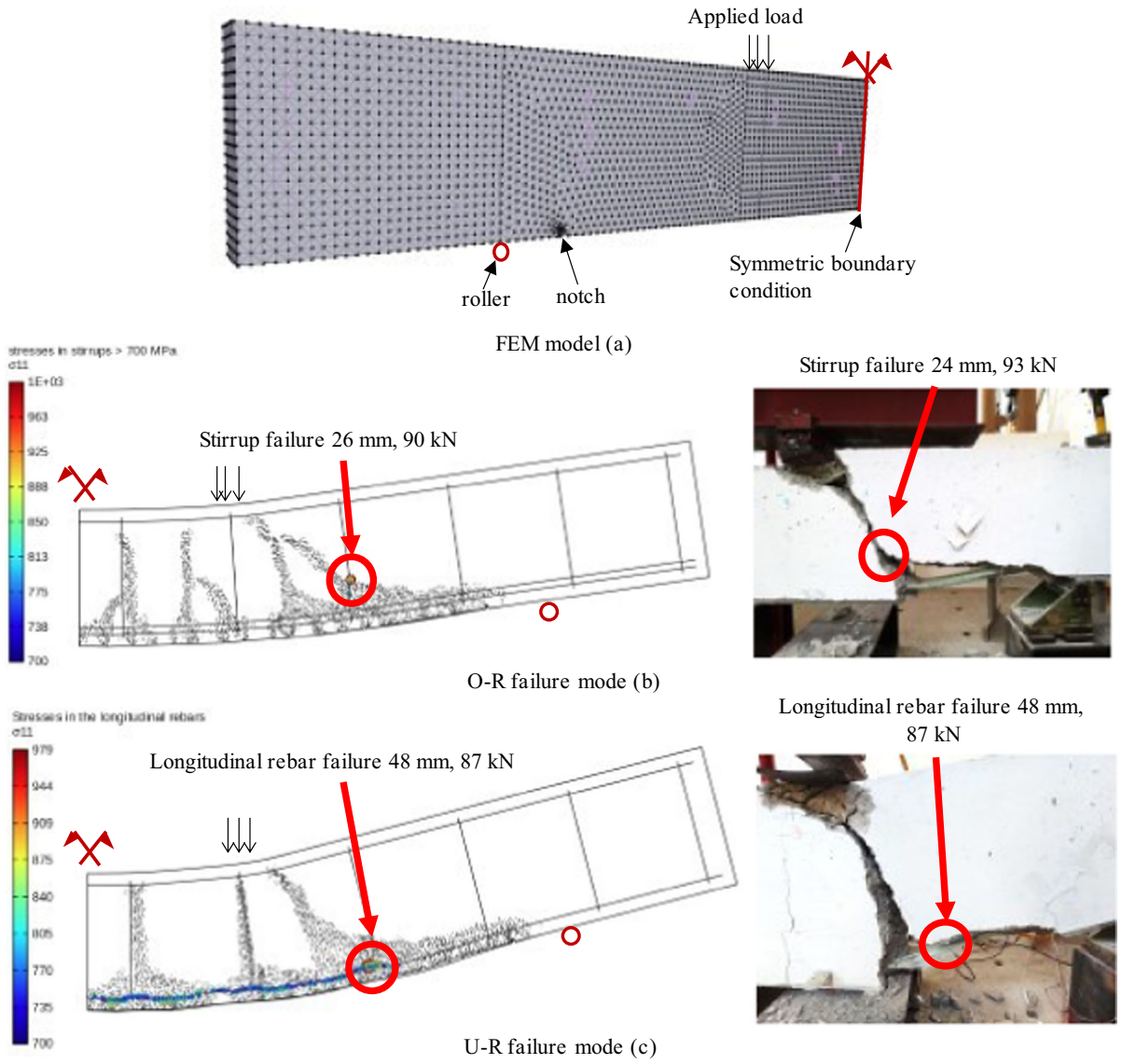

Fig. 7 Numerical model, mesh discretization and boundary conditions (**a**), comparison of numerical and experimental failure mode of O-R (**b**) and U-R specimens (**c**)

with the experimental strength of ben bars—f_{fr} in Table 4—presents a more contained variability).

Specifically, for the expected value, the dispersion of V_c is up to 27% (for U-R) and up to 22% for the V_f (for U-R). A different scenario is obtained in the case where the design values are considered. The incremental longitudinal reinforcement ratio from UR to OR increases the height of the neutral *y*-axis position (compressed concrete section) which leads to an increase in V_c strength. This is in good agreement with experimental evidence. Compared to a traditional steel reinforced section, with an equivalent bending reinforcement area, a section with FRP reinforcement presents a shallower neutral *y*-axis position because of the lower axial stiffness of FRP reinforcement. The crack width and extension are correspondingly greater. This element seems to encourage the use of FRP reinforcements joined to precompression.

4.1 Compressed concrete strength V_c

The technical standards analyzed consider the shear-bending interaction differently. ACI 440 R.15 and ACI 440–22 consider it through the $k(n_{fc}, \rho_f)$ and $k_r(n_{fc}, \rho_f)$ coefficient respectively, as shown in the "Appendix". Specifically, the incoming version of ACI 440–22 introduces the following changes (Table 1):

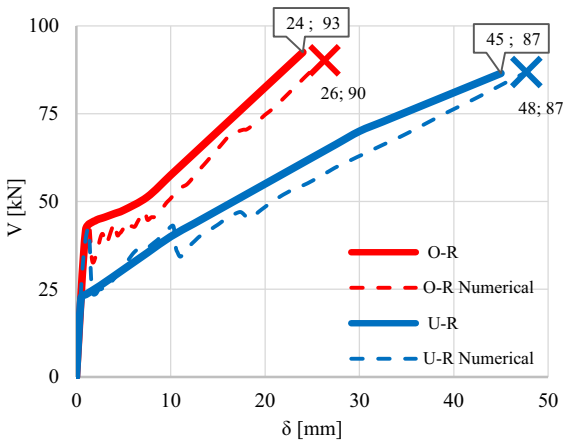

Fig. 8 V-δ curve of the O-R and U-R beam specimens: experimental and numerical data

- Two V_c expressions are given, with the indication to take the maximum value.
- λ_s coefficient is introduced (in line with the European approach). This penalizes the higher cross-section.

AFGC and CNR made ρ_f explicit in the expression of V_c. In AFGC, shear capacity depends on C_{rd}, k, ρ_f and n_{fs} while in CNR it depends on k, ρ_f and n_{fs}. The different V_c expressions of Table can be expressed as follows:

$$V_c = \tau \cdot b_w d \tag{8}$$

where τ usually depends on concrete compressive strength f_c, on longitudinal reinforcement ratio ρ_f, FRP modulus E_f and effective depth d (Eq. 9):

$$\tau = \tau\left(f_c'; \rho_f; E_f; d\right) \tag{9}$$

Therefore, τ takes the role of the average tension virtually acting on the area ($b_w \bullet d$), Eq. (10).

$$\tau = \frac{V_c}{b_w d} \tag{10}$$

Considering the geometry of the sample beams of this paper τ is plotted in Fig. 9 versus f_c and ρ_f.

CNR has proved to be the least conservative technical standard and the one that most encourages

Table 7 Average value and standard deviation of expected and design capacity of U-R beam and O-R beam calculated with [1–4]

Technical standard	Expected				Design			
	M (kNm)	V_c (kN)	V_f (kN)	V (kN)	M (kNm)	V_c (kN)	V_f (kN)	V (kN)
U-R beam								
ACI 440.1R15	82.5	16.8	48.0	64.9	38.0	10.5	9.4	19.9
ACI 440–22	82.5	25.0	48.0	73.1	38.0	15.6	11.8	27.3
AFGC	81.9	29.1	72.1	72.1	57.3	17.8	18.1	18.1
CNR	81.9	33.5	48.0	81.5	49.7	15.6	18.9	34.5
Average	82.2	26.1	54.0	72.9	45.7	14.9	14.5	25.0
St. Dev	0.3	7.1	12.0	6.8	9.5	3.1	4.7	7.5
% Dev	0%	27%	22%	9%	21%	21%	32%	30%
O-R beam								
ACI 440.1R15	113.8	23.6	49.4	73.0	59.5	14.7	9.7	24.4
ACI 440–22	113.8	25.6	49.4	75.0	59.5	15.9	12.1	28.0
AFGC	121.2	37.1	74.1	74.1	92.8	22.7	18.6	22.7
CNR	121.7	38.0	49.4	87.4	84.9	17.7	19.4	37.1
Average	117.7	31.1	55.6	77.4	74.2	17.7	14.9	28.0
St. Dev	4.4	7.5	12.4	6.7	17.2	3.5	4.8	6.4
% Dev	4%	24%	22%	9%	23%	20%	32%	23%

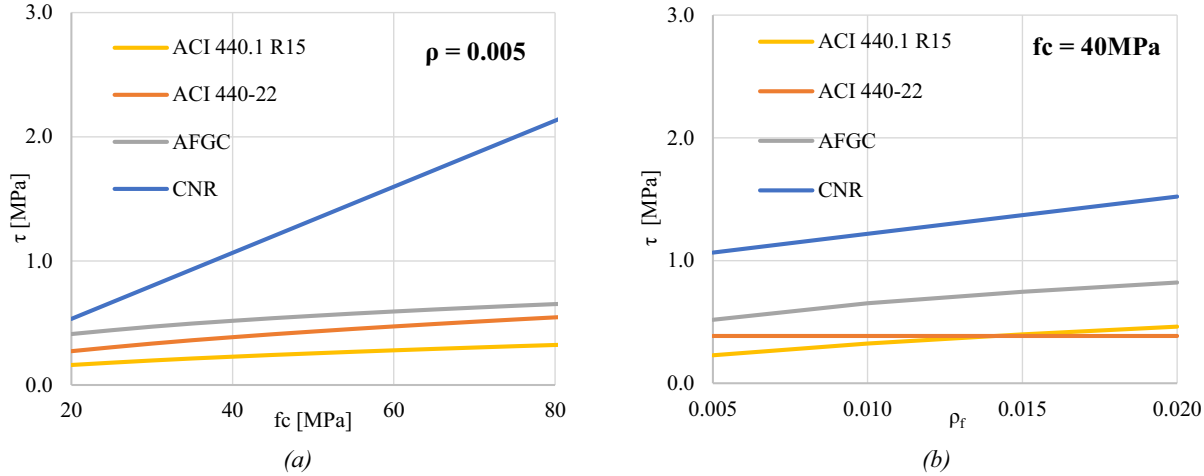

Fig. 9 τ versus f'_c (**a**) and α versus ρ_f (**b**). Expected values

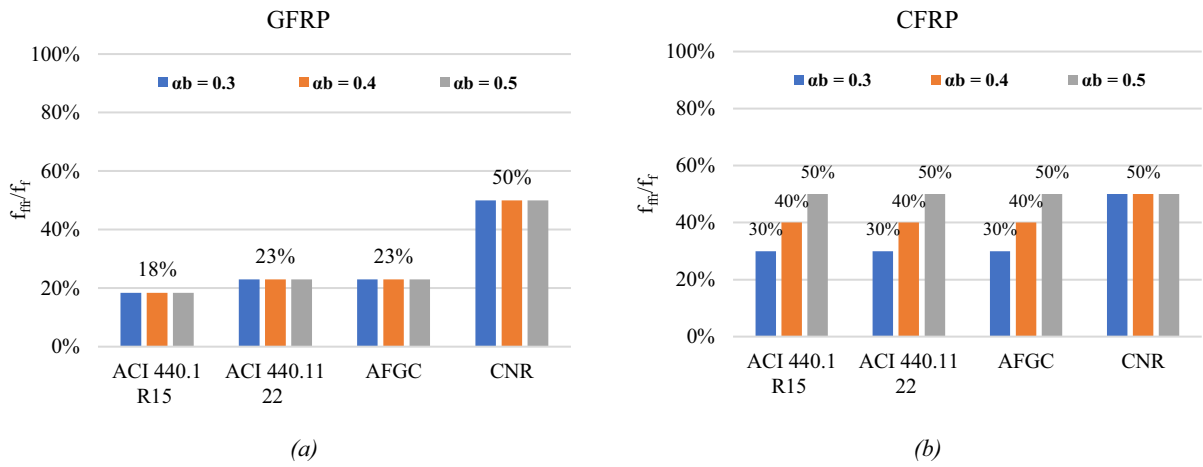

Fig. 10 f_{fr}/f_f for several bending coefficient α_b in case of GFRP and (**a**) CFRP (**b**) bars[3]. [3]—f_{fr}/f_f ratio is calculated using average values for f_f and E_f

the use of more performative concrete. The same can be observed by analyzing the V_c versus ρ_f graph. In CNR V_c depends on τ_r (f_{ct}) while in ACI and AFGC V_c depends on f_c. Here the value of f_{ct} derived from the Italian standard [f_{ct} = 0.3*f_c^(2/3)] was used, in agreement with the experimental calibration of CNR. It seems appropriate to perform further experimental investigations to improve the predictive reliability of V_c. This is of remarkable interest especially for beams with a reduced shear reinforcement A_{sw}/s, as for the sample beams of this work.

4.2 GFRP stirrups strength V_f

While the ACI and AFGC limited stress in transverse reinforcement to reduce crack width, the CNR only posited a mechanical limitation (f_{fr} = 0.5 f_f). This allows in CNR the use of fewer stirrups (and less restrictive limitation in stirrups spacing, Table 5). The f_{fr}/f_f ratio is graphed in Fig. 10 for Glass FRP (GFRP) and Carbon FRP (CFRP) bars for typical bending radius values. GFRP and CFRP are chosen for this comparison by having the lowest and highest values of elastic modulus in the range of commercial glass fiber

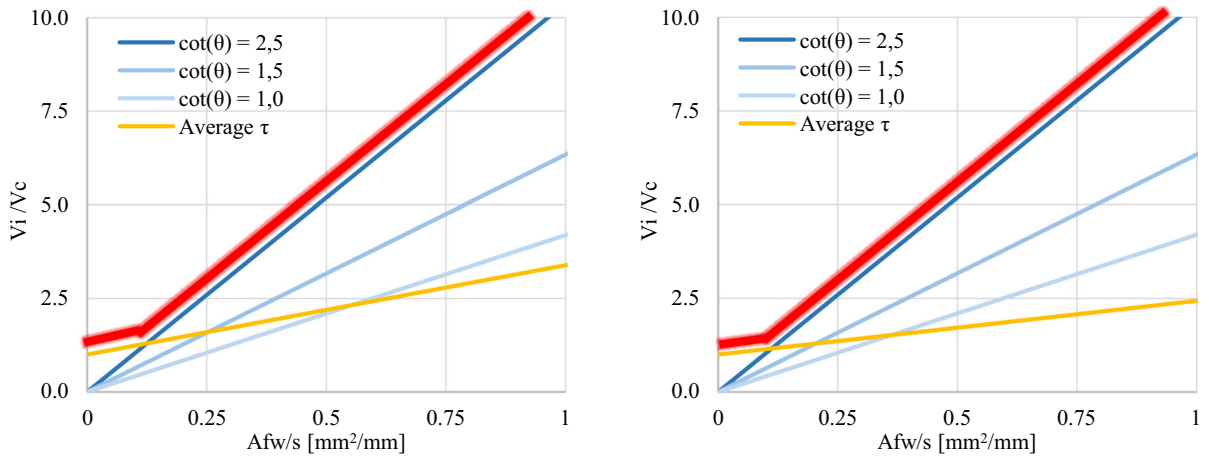

Fig. 11 V_i/V_c versus A_{sw}/s in case of $\rho_f = 0.01$ (**a**) and $\rho_f = 0.04$ (**b**)

bars, respectively. The strain limitation on f_{fr} (Table 1) produces a quite different value of f_{fr}/f_f ratio, having in practical application different rates of strength use. The strength reduction of Fig. 10 is calculated using the bending coefficient α_b of Eq. (5). For E_f and f_f average values from the literature are considered.

In the light of above findings, it is of significant interest to propose a synthesis approach between the two which is considered in the following paragraph.

4.3 Overall shear strength capacity V = V_c + V_f.

Looking at the histograms of Fig. 5 it appears that CNR produces the best estimation of the shear $V_{exp,}$ while AFGC and ACI underestimate it. Since V_c and V_f acted in parallel (Eq. 11), a strain limitation on f_{fr} is due to guarantee of the effective simultaneity of the two contributions of V_c and V_f. However, the current one (f_{fr} = 0.004 or 0.005 E_{fb}) appears quite conservative for the specimens analyzed in this work. On the other hand, the experimental campaign on bent bars carried out by Imjai et al. in 2017 [44] shows that the resistance of bent bars varies from 39 to 80% of the resistance of the straight bars (with a bending ratio $r_b/d \geq 3$, both for thermoplastic rather than for thermoset composites). So, the ratios from 18% up to 30% appear quite restrictive, in particular, if joined to the limitation $\theta = 45°$. A further release of the international standards should consider providing less scattered values both for V_c and V_f and a formally unitary analytical approach. Considering the limits above, the R-M approach with the current ones of ACI and CNR are compared. In R-M is excluded the limitation on the deformability of the stirrups since the term V_c is neglected. These two approaches are indicated in the following with subscripts 1 and 2. Considering Eq. (6) for V_c the expression V_1 and V_2 are:

$$V_1 = \frac{A_{fw} d}{s} \cot(\theta) f_{fr1} \tag{11}$$

with f_{fr1} is the experimental resistance of stirrups that can be in general expressed as a ratio of the resistance of the straight bar $f_{fr1} = \alpha_b f_f$.

$$V_2 = V_c + V_f \tag{12}$$

$$V_2 = b_w d \tau + \frac{A_{fw} d}{s} f_{fr2} \tag{13}$$

with f_{fr2} = min ($\alpha_E \cdot E_f$; $\alpha_b \cdot f_f$).

Equations (11) and (13) are shoved in Fig. 11. The shear capacity V_i is normalized concerning V_c. The V_i/V_c − (A_{fw}/s) lines are graphed considering in V_c τ = 0.6 MPa (for ρ_f = 0.01) and τ = 1.0MP for (ρ_f = 0.04), f_c = 40 MPa. In V_1 α_b = 0.5 (as in the approach of CNR) is chosen. The experimental value of α_b is 0.7.

Matching Eqs. (11) and (12), neglecting the terms α_E with respect to $\alpha_b \bullet \cot(\theta)$, and explicating A_{fw}/s is obtained:

$$\left(\frac{A_{fw}}{s}\right)^{*} = \frac{b_w}{(\alpha \cdot \cot(\theta))} \frac{\tau}{f_f} \tag{14}$$

$(A_{fw}/s)^{*}$, graphically represented by the intersection of the yellow and the shades of blue lines, is the stirrups amount from which V_2 produced a smaller value concerning V_1. It is also possible to calculate a defined stirrup amount that determines which one of the two methods is less conservative. $(A_{fw}/s)^{*}$ in the considered experimental campaign assuming the value 0.118 mm^2/mm in case of τ = 0.6 MPa and 0.281 mm^2/m in case of τ = 1.0 MPa, being 0.196 mm^2/mm the stirrups amount of the sample beams. The anticipated shear capacity of the specimens under consideration, as calculated using Eq. (11) with $\cot(\theta)$ = 1.5, assumes the value V_e = 76.1 kN (V_e/V_{exp} = 82% for OR and 88% for UR specimens). It's noteworthy that this value is slightly higher than those obtained by ACI and AFGC for UR cases and nearly identical to those obtained for OR (Table 7). So, if $A_{fw}/s \geq (A_{fw}/s)^{*}$ the approach (1), although based on prudent values of f_{fr1}, is less conservative and may be used for better material utilization (even neglecting the V_c terms). This is also allowed in practical cases by the corrosion resistance of FRP reinforcement that consents to defer the limitation on crack width to the serviceability limit states design scenarios, without implicating V_c and f_{fr2} reduction at the Ultimate Limit State. Considering the minimum shear reinforcement of Table 2 (0.172 mm^2/m) it turns out that approach (2) produces, in general, conservative results with respect to approach (1). This produces practical implications in structural design.

5 Conclusion

In this paper, the results of an experimental campaign carried out on GFRP-reinforced concrete beams, with a reduced amount of shear reinforcement, were compared with the shear capacity formulations of the American ACI (version of 2022 and previous), the French AFGC, and the Italian CNR. The comparison between the three analyzed standards has shown that:

- The bending capacity expression M of the analyzed standards produced consistent results, with a reduced deviation, under the 4% in the case that the expected values are considered (and up to 23% in case of design value).
- Despite the limited quantity of stirrups used in the current case studies, following standard guidelines, they should be analyzed as beams without explicit shear reinforcement. However, the experimental tests reveal a failure mechanism and a corresponding failure load that is characteristic of shear-reinforced beams.
- ACI, AFGC, and CNR standards expressions are applied to the illustrated case of study, and it is shown that the current standard formulae always underestimate the shear capacity of the prototypes (min 25%, max 6%);
- The shear capacity expression of the analyzed standards produced a deviation from 9% (in case of expected value) to 30% (in case of design values). The design values of shear capacity V are between 9 and 30% for U-R and between 9 and 23% for O-R. The CNR code produces a major estimation of shear capacity both for the design and for expected values.
- The calculation of V_c is carried out with different formulas leading to scattered results (up to 27%). This indicates that further investigations should be pursued, particularly for beams without or with reduced shear reinforcement.

The parametric analysis carried out joined to the experimental evidence on the two cases of study, consent to highlights the following points:

- Specimen failure modes and FEM models show that, after the first shear crack is formed, the strut will reorient (even with widely spaced stirrups and for under-reinforced beams) as long as an adequate bond length is ensured for the bending reinforcement.
- Considering the inclination θ of the compressed strut (as in AFGC), could improve the predictive ability of the V_f, expression. In ACI V_f is penalized by the reduction of f_{fr} (f_{fr} = 0.005 E_f means $f_{fr} \approx 0.2\ f_{fb}$ in case of GFRP). Taking into account the inclination θ of the compressed strut and following the physical-based R.M. approach (also confirmed from the experimental evidence), can be useful to obtain less conservative V_f estimation. This can be useful, especially for prestressed structures and in the case of thermoplastic GFRP bars where the reduction of strength in stirrups due

to bent effect is less relevant (and as a consequence, a strain limitation appears quite restrictive).
- Assuming $\theta = 45°$ as in ACI and CNR and subsequently performing reverse calculations for α_E the obtained values fall within the range of 0.017–0.022, all of which are greater than 0.005. So, considering the data of the presented tests, a value of $\alpha_E = 0.010$, may provide precautionary but less conservative results. This finding is in line with the proposal of the precedent researchers [45–47] and should be evaluated by analyzing the data of a parametric experimental campaign.
- It may be useful for structural optimization to provide a different approach depending on the percentage of shear reinforcement, based on the limit value of $(A_{fw}/s)^*$ (Eq. 14 in Sect. 4.3). This is of particular interest in the case of prestressed structures (where $\theta < 45°$ can be affordably assumed).
- FEM models with the programs SKTO developed by ASDEA and Opensees, tuned on experimental data, are able to accurately reproduce the experimental behavior and can be used in structural optimization.

This element represents an enhancing step between a better optimization of the material and a more physical and mechanical analytical expression.

The discussion of safety factors, which do vary among the different codes analyzed, falls outside the scope of this work. Instead, the proposal here is to consider adopting a distinct reduction coefficient that can more effectively account for the reduced resistance of GFRP stirrups (f_{fr}) in the studied case. With this approach, it becomes possible to reconsider the design capacity by utilizing Eqs. (11) and (13), aiming for material optimization as elaborated in Sect. 4.3.

It's worth highlighting the significance of this research, as underscored by the observed variability in the analytical approaches presented here, especially concerning V_f. In this regard, further experiments and parametric investigation are being conducted to explore the diverse shear resistance mechanisms in prototypes reinforced with varying percentages of longitudinal reinforcement and different stirrup area and spacing percentages.

Acknowledgements The authors would like to express their special thanks to SIREG GEOTECH (Italy) for providing technical data and the *Glasspree* GFRP bars used for testing and to the technical staff of the Laboratory of Materials and Construction of the University of Cagliari, and its spin-off Secured Solutions, for the special support in managing the experimental test.

Funding Open access funding provided by Università degli Studi di Cagliari within the CRUI-CARE Agreement.

Appendix

Clarification

For safety factors see the respective technical codes [1–4].

The strength of concrete is characterized by experimental tests. The strength G-FRP bars used are statistically characterized in [37] by furnishing the average (X_a) and the standard deviation (σ).

From this, the characteristic values (X_c) are calculated.

X_c corresponds to the 5.0th normal distribution for the European (Italian and French) standard and the 0.1th normal distribution for the North American Standard. So, being σ the standard deviation value, according to the European approach:

$$X_k = X_a - 1.6\sigma \tag{15}$$

While, according to the North American approach:

$$X_k = X_a - 3.0\sigma \tag{16}$$

About the subscript can be useful to clarify:

e expected (average material strength, no safety factors).

n nominal – from ACI – (characteristic material strength, no safety factors).
d design (characteristic material strength, and safety factors).

Equations

The expressions not explicitly illustrated in the paper can be found below. The value of k in ACI, AFGC, and CNR assumes a different expression:

ACI 440.1 R15 [1]

$$k = \sqrt{2\rho_f n_{fc} + \left(\rho_f n_{fc}\right)^2} - \rho_f n_{fc} \tag{17}$$

$$n_{fc} = \frac{E_f}{E_c} \tag{18}$$

ACI 440–22 [2]

$$k_{cr} = k = \sqrt{2\rho_f n_{fc} + \left(\rho_f n_{fc}\right)^2} - \rho_f n_{fc} \tag{19}$$

$$\lambda_s = \begin{cases} \sqrt[2]{2/(1+d/254)} \le 1.0 & A_{fw} < A_{fw,\min} \\ 1.0 & A_{fw} \ge A_{fw,\min}; \end{cases} \tag{20}$$

$$n_{fc} = \frac{E_f}{E_c} \tag{21}$$

$$\rho_f = \frac{A_f^+}{b_w d} \tag{22}$$

AFGC [3]

$$C_{Rd} = \frac{0.18}{\gamma_c} \tag{23}$$

$$k = \min\left\{ \frac{2}{1 + \sqrt[2]{200/d}} \right. \tag{24}$$

CNR [4]

$$\tau_R = 0.25 f_{ct} \tag{25}$$

$$k = \begin{cases} 1.6 - d & A_{fw} < A_{fw,\min} \\ 1.0 & A_{fw} \ge A_{fw,\min}; \end{cases} \tag{26}$$

References

1. ACI (American Concrete Institute) (2015) Guide for the design and construction of structural concrete reinforced with FRP bars. ACI, Farmington Hills, MI: ACI
2. ACI (American Concrete Institute) (2022) Building code requirements for structural concrete reinforced with glass fiber-reinforced polymer (GFRP) bars. Farmington Hills, MI: ACI
3. Association Française de Génie Civil (AFGC) Utilisation d'armatures composites (à fibres longues et à matrice organique) pour le béton armé
4. CNR (National Research Council) (2007) Guide for the design and construction of concrete structures reinforced with fiber-reinforced polymer bars. Italian National Research Council (CNR) - Advisory committee on technical recommendations for construction
5. Camata G, Spacone E, Zarnic R (2007) Experimental and nonlinear finite element studies of RC beams strengthened with FRP plates. Compos B Eng 38:277–288. https://doi.org/10.1016/j.compositesb.2005.12.003
6. Ceroni F, Cosenza E, Gaetano M, Pecce M (2006) Durability issues of FRP rebars in reinforced concrete members. Cem Concr Compos 28:857–868. https://doi.org/10.1016/j.cemconcomp.2006.07.004
7. Xiao J, Qiang C, Nanni A, Zhang K (2017) Use of sea-sand and seawater in concrete construction: current status and future opportunities. Constr Build Mater 155:1101–1111. https://doi.org/10.1016/j.conbuildmat.2017.08.130
8. Santarsiero G, Masi A, Picciano V (2021) Durability of gerber saddles in RC bridges: analyses and applications (Musmeci Bridge, Italy). Infrastructures (Basel) 6:1–23. https://doi.org/10.3390/infrastructures6020025
9. Stochino F, Fadda ML, Mistretta F (2018) Low cost condition assessment method for existing RC bridges. Eng Fail Anal 86:56–71. https://doi.org/10.1016/J.ENGFAILANAL.2017.12.021
10. Collins MP, Mitchell N (1980) Design proposals for shear and torsion. J Prestress Concr Inst 25:70
11. Wegian FM, Abdalla HA (2005) Shear capacity of concrete beams reinforced with fiber reinforced polymers. Compos Struct. https://doi.org/10.1016/j.compstruct.2004.10.001
12. Ghani RA, Isgor BO, Greenaway S, Alistair S (2004) Concrete contribution to the shear resistance of fiber reinforced polymer reinforced concrete members. J Compos Constr 8:452–460. https://doi.org/10.1061/(ASCE)1090-0268(2004)8:5(452)

13. Razaqpur AG, Spadea S (2015) Shear strength of FRP reinforced concrete members with stirrups. J Compos Constr. https://doi.org/10.1061/(asce)cc.1943-5614.0000483
14. Tureyen AK, Frosch RJ (2003) Concrete shear strength: another perspective. ACI Struct J. https://doi.org/10.14359/12802
15. Fico R, Prota A, Manfredi G (2008) Assessment of Eurocode-like design equations for the shear capacity of FRP RC members. Compos B Eng 39:792–806. https://doi.org/10.1016/J.COMPOSITESB.2007.10.007
16. Oller E, Marí A, Bairán JM, Cladera A (2015) Shear design of reinforced concrete beams with FRP longitudinal and transverse reinforcement. Compos B Eng 74:104–122. https://doi.org/10.1016/J.COMPOSITESB.2014.12.031
17. Nehdi M, El Chabib H, Aly SA (2007) Proposed shear design equations for FRP-reinforced concrete beams based on genetic algorithms approach. J Mater Civ Eng 19:1033–1042. https://doi.org/10.1061/(ASCE)0899-1561(2007)19:12(1033)
18. Mukhtar F, Deifalla A (2023) Shear strength of FRP reinforced deep concrete beams without stirrups: test database and a critical shear crack-based model. Compos Struct. https://doi.org/10.1016/j.compstruct.2022.116636
19. Deitz DH, Gesund IEH (1999) One-way slabs reinforced with glass fiber reinforced polymer reinforcing bars, vol 188. Special Publication, pp 279–286
20. Michaluk CR, Rizkalla SH, Tadros G, Benmokrane B (1998) Flexural behavior of one-way concrete slabs reinforced by fiber reinforced plastic reinforcements. ACI Struct J 95:353–365. https://doi.org/10.14359/552
21. El-Sayed AK (2006) Concrete contribution to the shear resistance of frp-reinforced concrete beams
22. Hegger J, Niewels J, Kurth M (2009) Shear analysis of concrete members with fiber- reinforced polymers (FRP) as internal reinforcement. In: The international symposium on fibre- reinforced polymer reinforcement for concrete structures, FRPRCS-9. University of Adelaide - Oehlers, Deric John. and Griffith, M. C. and Seracino, R., Sydney, Australia
23. Bentz E, Massam L, Collins M (2010) The shear strength of large concrete members with FRP reinforcement. J Compos Constr. https://doi.org/10.1061/(ASCE)CC.1943-5614.0000108
24. Hoult NA, Sherwood EG, Bentz EC, Collins MP (2008) Does the use of FRP reinforcement change the one-way shear behavior of reinforced concrete slabs? J Compos Constr 12:125–133. https://doi.org/10.1061/ASCE1090-0268200812:2125
25. Ebid AM, Deifalla A (2021) Prediction of shear strength of FRP reinforced beams with and without stirrups using (GP) technique. Ain Shams Eng J 12:2493–2510. https://doi.org/10.1016/j.asej.2021.02.006
26. Bashir R, Ashour A (2012) Neural network modeling for shear strength of concrete members reinforced with FRP bars. Compos B Eng 43:3198–3207. https://doi.org/10.1016/j.compositesb.2012.04.011
27. Lee S, Lee C (2014) Prediction of shear strength of FRP-reinforced concrete flexural members without stirrups using artificial neural networks. Eng Struct 61:99–112. https://doi.org/10.1016/J.ENGSTRUCT.2014.01.001
28. Pecce M, Manfredi G, Cosenza E (2000) Experimental response and code models of GFRP RC beams in bending. J Compos Constr 4:182–190. https://doi.org/10.1061/(ASCE)1090-0268(2000)4:4(182)
29. Frosch AKT, Frosch RJ (2003) Concrete shear strength: another perspective. ACI Struct J. https://doi.org/10.14359/12802
30. Aiello MA, Leone M, Pecce M (2007) Bond performances of FRP rebars-reinforced concrete. J Mater Civ Eng 19:205–213. https://doi.org/10.1061/(ASCE)0899-1561(2007)19:3(205)
31. Galati N, Nanni A, Dharani LR et al (2006) Thermal effects on bond between FRP rebars and concrete. Compos Part A Appl Sci Manuf 37:1223–1230. https://doi.org/10.1016/j.compositesa.2005.05.043
32. Guadagnini M, Pilakoutas K, Waldron P (2006) Shear resistance of FRP RC beams: experimental study. J Compos Constr 10:464–473. https://doi.org/10.1061/(ASCE)1090-0268(2006)10:6(464)
33. AA.VV. (2007) FRP reinforcement in RC structures. fédération internationale du béton, (fib), Stuttgart
34. Ehsani MR, Saadatmanesh H, Tao S (1995) Bond of hooked glass fiber reinforced plastic (GFRP) reinforcing bars to concrete. ACI Mater J 92:391–400
35. A.A. (1992) EN 1992-1-1 Eurocode 2: Design of concrete structures - Part 1–1: General rules and rules for buildings. EUROPEAN STANDARD, Avenue Marnix 17, B-1000 Brussels
36. AA. VV. (2018) Norme tecniche per le costruzioni 2018 (NTC 2018). Ministero delle Infrastrutture e dei trasporti, Roma
37. Kocaoz S, Samaranayake VA, Nanni A (2005) Tensile characterization of glass FRP bars. Compos B Eng 36:127–134. https://doi.org/10.1016/J.COMPOSITESB.2004.05.004
38. ASTM (2022) D7957/D7957M−22: Standard Specification for Solid Round Glass Fiber Reinforced Polymer Bars for Concrete Reinforcement. ASTM International, 100 Barr Harbor Drive, PO Box C700, West Conshohocken, PA 19428-2959. United States
39. Camata G (2022) STKO Scientific ToolKit for OpenSees. https://asdea.eu/software/about-stko/. Accessed 4 Jun 2023
40. McKenna F (2011) OpenSees: a framework for earthquake engineering simulation. Comput Sci Eng 13:58–66. https://doi.org/10.1109/MCSE.2011.66
41. Petracca M (2022) ASDConcrete3D Material. https://opensees.github.io/OpenSeesDocumentation/user/manual/material/ndMaterials/ASDConcrete3D.html. Accessed 4 Jun 2023
42. Petracca M, Camata G, Spacone E, Pelà L (2022) Efficient constitutive model for continuous micro-modeling of masonry structures. Int J of Arch Herit 17:1–13. https://doi.org/10.1080/15583058.2022.2124133
43. AA.VV. (2013) FIB | Model code for concrete structures 2010. Wiley-VCH Verlag GmbH & Co. KGaA, Weinheim, Germany
44. Imjai T, Guadagnini M, Pilakoutas K (2017) Bend strength of FRP Bars: experimental investigation and bond modeling. J Mater Civ Eng. https://doi.org/10.1061/(ASCE)
45. Duranovic N, Pilakoutas K, Waldron P (1997) Tests on concrete beams reinforced with glass fibre reinforced plastic

bars. In: Third international symposium of non-metallic (FRP) reinforcement for Concrete Structures (FRPRCS-3). Sapporo Japan, pp 527–534
46. Tottori S, Wakui H (1993) Shear Capacity of RC and PC Beams Using FRP Reinforcement. In: SP-138: Fiber-reinforced-plastic reinforcement for concrete structures - international symposium. American Concrete Institute, pp 615–632
47. Yost JR, Gross SP, Dinehart DW (2001) Shear strength of normal strength concrete beams reinforced with deformed GFRP bars. J Compos Constr 5:268–275. https://doi.org/10.1061/(ASCE)1090-0268(2001)5:4(268)